

Upper bounds on the low-frequency stochastic gravitational wave background from pulsar timing observations: current limits and future prospects

F. A. Jenet¹, G. B. Hobbs², W. van Straten¹, R. N. Manchester², M. Bailes³, J. P. W. Verbiest^{2,3}, R. T. Edwards², A. W. Hotan⁴, J. M. Sarkissian², S. M. Ord⁵

ABSTRACT

Using a statistically rigorous analysis method, we place limits on the existence of an isotropic stochastic gravitational wave background using pulsar timing observations. We consider backgrounds whose characteristic strain spectra may be described as a power-law dependence with frequency. Such backgrounds include an astrophysical background produced by coalescing supermassive black-hole binary systems and cosmological backgrounds due to relic gravitational waves and cosmic strings. Using the best available data, we obtain an upper limit on the energy density per unit logarithmic frequency interval of $\Omega_g^{\text{SMBH}}(1/8 \text{ yr})h^2 \leq 1.9 \times 10^{-8}$ for an astrophysical background which is five times more stringent than the earlier Kaspi et al. (1994) limit of 1.1×10^{-7} . We also provide limits on a background due to relic gravitational waves and cosmic strings of $\Omega_g^{\text{relic}}(1/8 \text{ yr})h^2 \leq 2.0 \times 10^{-8}$ and $\Omega_g^{\text{cs}}(1/8 \text{ yr})h^2 \leq 1.9 \times 10^{-8}$ respectively. All of the quoted upper limits correspond to a 0.1% false alarm rate together with a 95% detection rate. We discuss the physical implications of these results and highlight the future possibilities of the Parkes Pulsar Timing Array project. We find that our current results can 1) constrain the merger rate of supermassive binary black hole systems at high red shift, 2) rule out some relationships between the black hole mass and the galactic halo mass, 3) constrain the rate of expansion in the inflationary era and 4) provide an upper bound on the dimensionless tension of a cosmic string background.

¹Center for Gravitational Wave Astronomy, University of Texas at Brownsville, TX 78520 (merlyn@phys.utb.edu)

²Australia Telescope National Facility, CSIRO, PO Box 76, Epping NSW 1710, Australia

³Centre for Astrophysics and Supercomputing, Swinburne University of Technology, P. O. Box 218, Hawthorn VIC 3122, Australia

⁴Physics Department, University of Tasmania, Hobart, TAS 7001, Australia

⁵School of Physics, University of Sydney, NSW 2006, Australia

Subject headings: pulsars: general — gravitational waves — methods: data analysis — early universe — Galaxies: statistics

1. Introduction

Pulsar timing observations (see Lorimer & Kramer 2005, Edwards, Hobbs & Manchester 2006 for a review of the techniques) provide a unique opportunity to study low-frequency ($10^{-9} - 10^{-7}$ Hz) gravitational waves (GWs) (e.g., Sazhin 1978, Detweiler 1979, Bertotti, Carr, & Rees 1983, Foster & Backer 1990, Kaspi, Taylor & Ryba 1994, Jenet et al. 2005). Sources in this low-frequency band include binary supermassive black holes, cosmic superstrings, and relic gravitational waves from the Big Bang (Jaffe & Backer 2003, Maggiore 2000).

An isotropic stochastic background can be described by its characteristic strain spectrum $h_c(f)$ which, for most models of interest, may be written as a power-law dependence on frequency, f :

$$h_c(f) = A \left(\frac{f}{\text{yr}^{-1}} \right)^\alpha. \quad (1)$$

Table 1 shows the expected values of A and α for different types of stochastic backgrounds that have been addressed in the literature. The characteristic strain is related to the one-sided power spectrum of the induced timing residuals, $P(f)$, as

$$P(f) = \frac{1}{12\pi^2} \frac{1}{f^3} h_c(f)^2, \quad (2)$$

and to $\Omega_{gw}(f)$, the energy density of the background per unit logarithmic frequency interval, as

$$\Omega_{gw}(f) = \frac{2}{3} \frac{\pi^2}{H_0^2} f^2 h_c(f)^2 \quad (3)$$

where H_0 is the Hubble constant. Note that the one-sided power spectrum, $P(f)$, is defined so that

$$\int_0^\infty P(f) df = \sigma^2 \quad (4)$$

where σ^2 is the variance of the arrival time fluctuations, or timing residuals, generated by the presence of the GW background. Since σ^2 has the physical units of s^2 , $P(f)$ has the units of s^2/Hz or s^3 .

Jenet et al. (2005) developed a technique to make a definitive detection of a stochastic background of GWs by looking for correlations between pulsar observations. It was shown

that approximately 20 pulsars would need to be observed with a timing precision of ~ 100 ns over a period of 5 years in order to make such a detection if the GW background is at the currently predicted level (Jaffe & Backer 2003, Wyithe & Loeb 2003, Enoki et al. 2004, Sesana et al. 2004). The Parkes Pulsar Timing Array (PPTA) project (Hobbs 2005) is trying to achieve these ambitious goals, but the currently available data-sets do not provide the required sensitivity for a detection. In this paper, we introduce a method to place an upper bound on the power of a specified stochastic GW background using observations of multiple pulsars. Full technical details of our implementation will be published in Hobbs et al. (2006). Here, this method is applied to data (see Section 2) from seven pulsars observed for the PPTA project combined with an earlier publicly available data-set.

Upper limits have already been placed on the amplitude of any such background of GWs. Using eight years of observations for PSR B1855+09, Kaspi et al. (1994) obtained a limit of $\Omega_g h^2 \leq 1.1 \times 10^{-7}$, where $H_0 = 100h$ km s $^{-1}$ Mpc $^{-1}$, at the 95% confidence level¹ for the case when $\alpha = -1$ (i.e. Ω_{gw} is independent of frequency). This work was continued by Lommen (2002) who used 17 yrs of observations to obtain $\Omega_g h^2 < 2 \times 10^{-9}$. However, the statistical method used for both of these analyses has been criticized in the literature (see, for instance, Thorsett & Dewey 1996, McHugh et al. 1996, Damour & Vilenkin 2005). In this paper, we develop a frequentist technique, similar to that used by the LIGO science collaboration (Abbott et al. 2006), to place an upper bound on A , given α . The technique makes use of a statistic, Υ , defined below, which is sensitive to red noise in the pulsar timing residual data. Upper bounds on A are determined using Υ together with a specified false alarm rate, \mathcal{P}_f , and detection rate, \mathcal{P}_d . Monte-Carlo simulations are used to determine these probabilities by generating pulsar pulse times-of-arrival consistent with a GW background. All of the upper limits quoted in this paper correspond to $\mathcal{P}_f = 0.1\%$ and $\mathcal{P}_d = 95\%$.

¹Their more stringent constraint of $\Omega_g h^2 \leq 6 \times 10^{-8}$ was obtained when data from PSRs B1855+09 and B1937+21 were combined. Since the data from PSR B1937+21 is far from white, we believe this limit is artificially low and therefore restrict our discussion to the PSR B1855+09 data only.

Table 1: The expected parameters for predicted stochastic backgrounds

Model	A	α	References
Supermassive black holes	$10^{-15} - 10^{-14}$	$-2/3$	Jaffe & Backer (2003) Wyithe & Loeb (2003) Enoki et al. (2004)
Relic GWs	$10^{-17} - 10^{-15}$	$-1 - -0.8$	Grishchuk (2005)
Cosmic String	$10^{-16} - 10^{-14}$	$-7/6$	Maggiore (2000)

2. Observations

We expect the isotropic background to generate timing residuals with a “red” spectrum: a spectrum with excess power at low frequencies or, equivalently, long time scale correlations in the residuals. Therefore, we have restricted our analysis to those pulsars having formally white spectra: a spectrum with statistically equal power at all frequencies or no correlations in the residuals. This allows us to put the best upper limit on the background by bounding the level of any red process in those data sets. Three separate tests were used in order to determine the statistical properties of the data and to select data-sets that are statistically white. First, the normalized Lomb-Scargle periodogram was calculated for each residual time series. No significant peaks were seen in any of the data used. Second, the variance of the residuals was shown to decrease as $1/n$ where n is the number of adjacent time samples averaged together. If the data were correlated the variance would not scale as $1/n$. Third, no significant structures were seen in the polynomial spectrum (defined below) for each individual spectrum or in the averaged spectrum. Note that the publicly available data-set for PSR B1937+21 (Kaspi et al. 1994) was not used in our analysis since its timing residuals do not pass these three tests.

We made use of the following data-sets which passed the tests: 1) observations of PSR B1855+09 (also known as PSR J1857+0943) from the Arecibo radio telescope that are publicly available (Kaspi et al. 1994), 2) observations for PSRs B1855+09, J0437–4715, J1024–0719, J1713+0747, J1744–1134, J1909–3744 and B1937+21 (J1939+2134) using the Parkes radio telescope and reported by Hotan et al. (2006) and 3) recent observations of all of these pulsars made as part of the PPTA and related Swinburne timing projects. The Kaspi et al. (1994) data-set was obtained at ~ 1400 MHz over a period of 8 yrs. The PPTA observations, which commenced in February 2004, include ~ 20 millisecond pulsars and use the 10/50-cm dual-frequency receiver and a 20-cm receiver at the Parkes radio telescope. Each pulsar is typically observed at all three frequencies in sessions at intervals of 2 – 3 weeks. The results used here were obtained using a correlator with 2-bit sampling capable of bandwidths up to 1 GHz and a digital filterbank system with 8-bit sampling of a 256 MHz bandwidth. The PPTA observations and the earlier Hotan et al. (2006) data-sets also used the Caltech Parkes Swinburne Recorder 2 (CPSR2 – see Hotan et al. 2006), a baseband recorder that coherently dedisperses two observing bands of 64 MHz bandwidth, centered on 1341 and 1405 MHz for observations at 20 cm and around 3100 MHz and 685 MHz for (simultaneous) observations with the coaxial 10/50 cm receiver. Full details of the PPTA project will be presented in a forthcoming paper; up-to-date information can be obtained

from our web-site². Unfortunately, our stringent requirements on the “whiteness” of the timing residuals has restricted the use of some of our nominally best-timing pulsars. For instance, even though a 10-yr data span is available for PSR J0437–4715, the full-length data-set is significantly affected by calibration and hardware-induced artifacts as well as other unknown sources of timing noise.

A listing of the pulsars observed, the observation span, number of points and weighted rms timing residual after fitting for the pulsars’ pulse frequency and its first derivative, astrometric and binary parameters are presented in Table 2. Arbitrary offsets have been subtracted between data-sets obtained with different instrumentation. Combining these data-sets provides us with data spans of ~ 20 yr for PSR B1855+09 and $\sim 2 - 4$ years for the remaining pulsars. The final timing residuals are plotted in Fig. 1.

3. New upper bounds on the stochastic backgrounds

The goal here is to use the measured timing residuals from multiple pulsars in order to determine the smallest value of A that can be detected for a given α as defined by equation 1. This is done in a three-step process. First, a detection algorithm is defined that is sensitive to the presence of the background. Second, this algorithm is tuned so that in the absence of a signal (i.e. $A = 0$), the probability of the detection scheme falsely detecting the background is set at \mathcal{P}_f , known as the false alarm rate. Lastly, for the given detection scheme and false alarm rate, the upper bound, A_{upper} , is chosen so that the probability of detecting a

²<http://www.atnf.csiro.au/research/pulsar/ppta>

Table 2: Pulsar observations used for this analysis

Pulsar	Telescope	Span (d)	N	rms residual (μs)
J0437–4715	Parkes	815	233	0.12
J1024–0719	Parkes	861	92	1.10
J1713+0747	Parkes	1156	168	0.23
J1744–1134	Parkes	1198	101	0.52
J1857+0943	Arecibo/Parkes	7410	398	1.12
J1909–3744	Parkes	866	2859	0.29
J1939+2134	Parkes	862	231	0.21

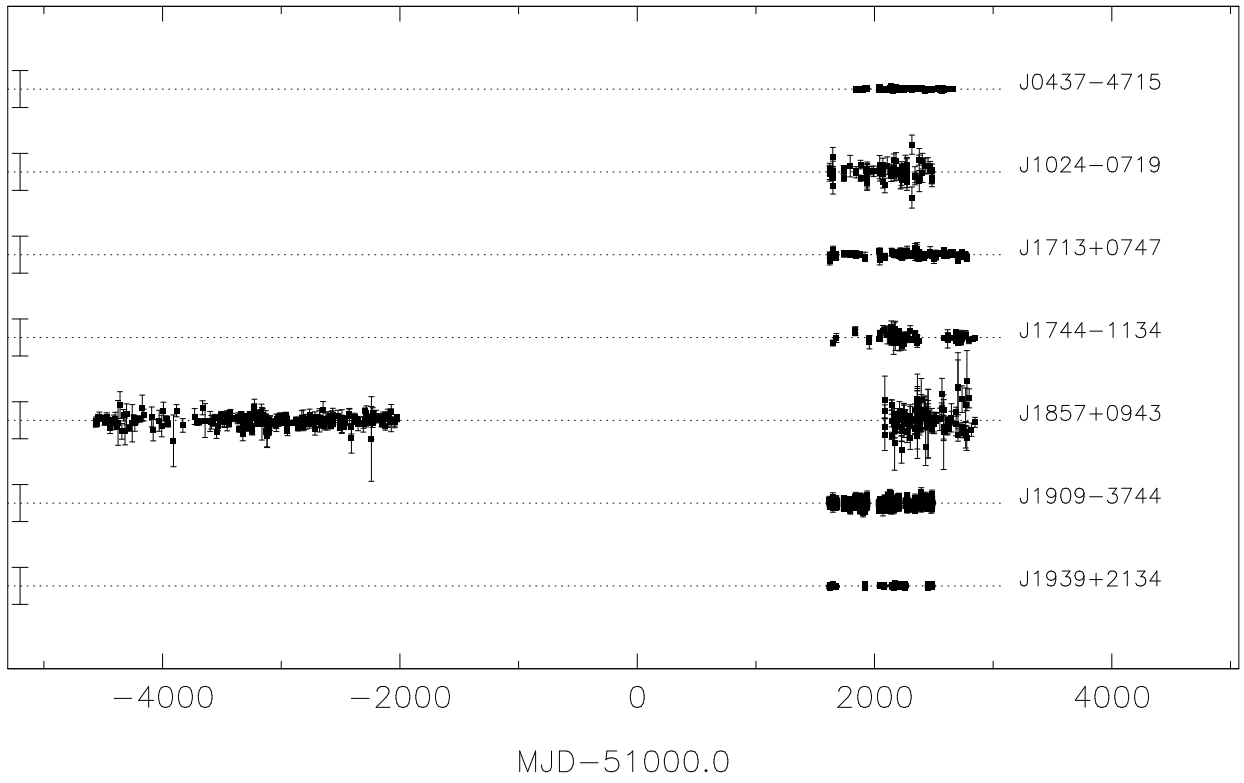


Fig. 1.— Pulsar timing residuals. The length of the vertical line on the left hand edge represents $10\mu s$.

background with $A = A_{\text{upper}}$ is \mathcal{P}_d . For this paper, the false alarm rate is set to 0.1% while the upper-bound detection rate is set to 95%.

Since all current models of the background predict that the induced timing residuals will be “red” (the spectrum increases at lower frequencies), the detection scheme employed here is defined to be sensitive to a red spectrum. The existence of a red spectrum in the timing residuals is therefore necessary, but not sufficient, evidence for the existence of a GW background. Hence, we can use a statistic sensitive to a red spectrum in order to place an upper bound on the amplitude of the characteristic strain spectrum. Since the data-sets are irregularly sampled and cover different time spans, a spectrum based on orthogonal polynomials is employed. Each pulsar data-set consists of n_p measured residuals, $x_p(i)$, a time tag $t_p(i)$, and an uncertainty $\sigma_p(i)$, where i is the data sample index and p is an index referring to a particular pulsar. The time tags are scaled so that normalized time tags, $\tau_p(i)$, run from -1 to 1 . These $\tau_p(i)$ values are used in a weighted Gram-Schmidt orthogonalization procedure to determine a set of orthonormal polynomials $j_p^l(i)$ defined from

$$\sum_{i=0}^{n_p-1} \frac{j_p^l(i)j_p^k(i)}{\sigma_p^2(i)} = \delta_{lk} \quad (5)$$

where $j_p^l(i)$ is the l 'th order polynomial evaluated at $\tau_p(i)$ and δ_{lk} is the standard Kronecker delta function. Note the highest power of t in $j_p^l(i)$ is l . For the case where τ is continuous and $\sigma_p^2(i) = 1$, the above sum becomes an integral and $j_p^l(i)$ become the familiar Legendre polynomials. The following coefficients are calculated using the orthonormal polynomials, $j_p^l(i)$, and the timing residuals $x_p(i)$:

$$C_p^l = \sum_{i=0}^{n_p-1} \frac{j_p^l(i)x_p(i)}{\sigma_p^2(i)}. \quad (6)$$

The pulsar average polynomial spectrum is given by

$$P_l = \sum_p \frac{(C_p^l)^2}{v_p} \quad (7)$$

where the weighted variance, v_p , is defined as $\frac{1}{n_p} \sum_{i=0}^{n_p-1} (x_p(i) - \bar{x}_p)^2 / \sigma_p^2(i)$ and \bar{x} is the mean of x . Since the stochastic background is red, P_l will be large for low values of l if the background significantly influenced the residuals. Hence, $\Upsilon = \sum_{l=0}^{l=7} P_l$ may be used as a statistic to detect the background. An upper limit of seven is used since 95% of the power is contained in the first seven polynomials for the case of $\alpha = -2/3$. The background will be “detected” if $\Upsilon > \Upsilon_0$ where Υ_0 is set so that the false-alarm rate is given by \mathcal{P}_f .

A Monte-Carlo simulation was used to determine Υ_0 and A_{upper} . Complete details of the simulation and its implementation may be found in Hobbs et al. (2006), but a brief overview is given here. The simulation, undertaken in the pulsar timing package TEMPO2 (Hobbs, Edwards & Manchester 2006), generates an ideal TOA data-set (with the same sampling as the observed data) from a measured set of TOAs and a given timing model. The fluctuations due to the GW background for a given A and α are introduced into the TOAs by adding together 10,000 sinusoidal GWs which come from random directions on the sky and have randomly chosen frequencies in the range $(1/2000\text{yr})$ – $(1/0.5\text{d})$. As a test of the simulation, the ensemble-averaged power spectrum of the simulated residuals was calculated over a time scale much larger than the longest GW timescale (i.e. 2000 years) and was shown to be consistent with equation 2 as expected. The GW residuals are then added to the ideal TOA data-set for each pulsar. In order to include the effects of measurement noise, the measured timing residuals are added back into the data-set, but randomly shuffled. This ensures that the added noise has the same probability distribution as the actual measurement noise. In this way, a new set of TOAs are generated that include both measurement noise and the GW background. Note that the shuffling procedure is only valid when the data have a white spectrum. Otherwise, the spectral properties of the original data set and the shuffled data set will not be the same. This simulated TOA data set will then be analyzed in exactly the same way as a real data set. Hence, all the systemic effects which inhibit gravitational wave detection such as low order polynomial removal, Earth’s orbital motion, annual parallax effects, and orbital companion effects are appropriately accounted for in the simulation.

To calculate Υ_0 , the simulation generates 10000 independent simulated sets of TOAs for each pulsar with $A = 0$ (i.e. no GW background). The statistic Υ is calculated for each of the 10000 trials. Using this set of Υ values together with the chosen false alarm rate, \mathcal{P}_f , the value of Υ_0 can be determined. Once Υ_0 is chosen, the simulation is used to generate TOA data-sets that include the effects of GWs. For a given value of A , the probability of detection is determined using Υ and Υ_0 . A_{upper} is chosen to be that value of A when the probability of detection is equal to \mathcal{P}_d .

Note that the effects of unknown time offsets (“jumps”) in the data-sets are included in the calculation of both Υ_0 and A_{upper} using this technique since TEMPO2 fits for these offsets in the TOA data-set after the GW background has been added. Since we are using TEMPO2 to analyze the data, the effects of all the fitting procedures are being taken into account.

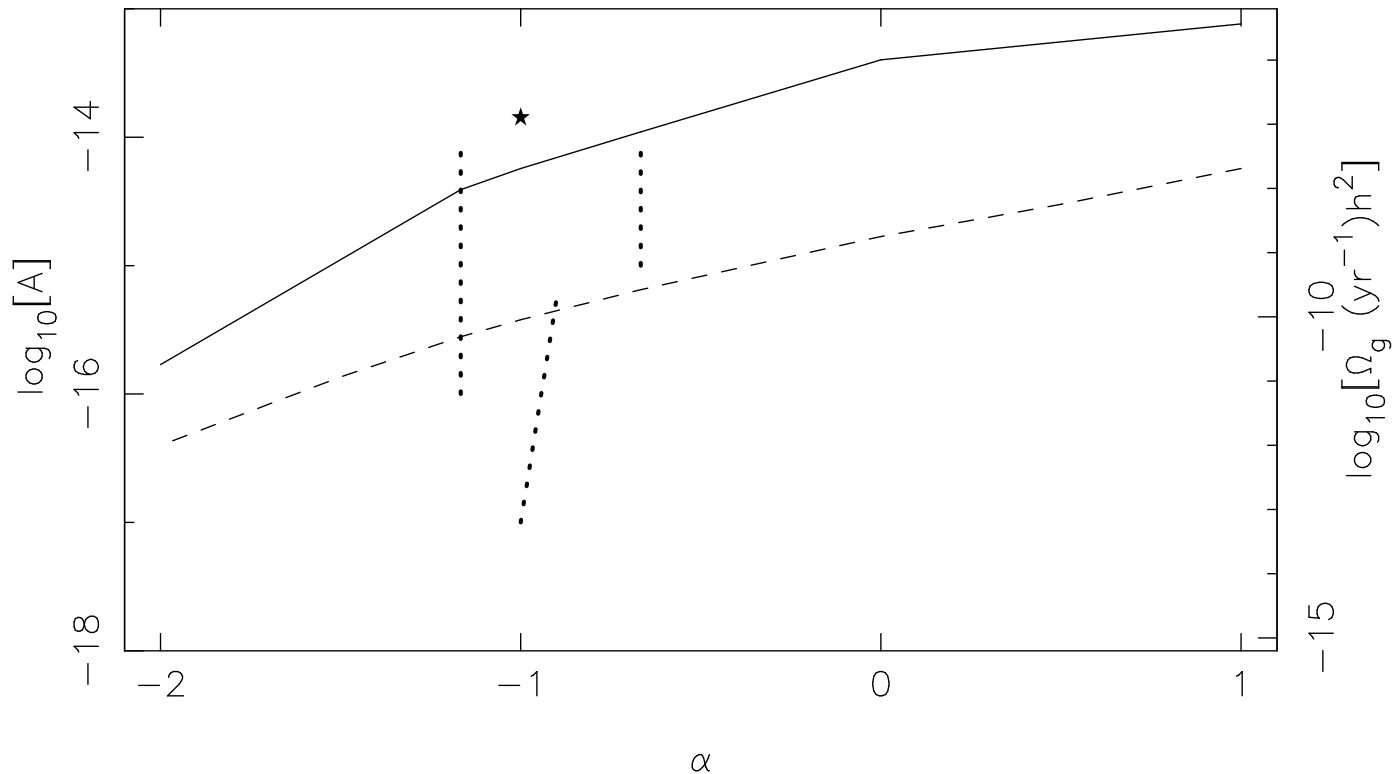


Fig. 2.— Minimum detectable A (or $\Omega_{gw}(1\text{yr}^{-1})h^2$ - right axis) versus α for our current limits (solid line) and potential future limits from the PPTA (dashed line). The star symbol indicates the limit obtainable using the Kaspi et al. (1994) observations of PSR B1855+09. From left to right the near-vertical dotted lines indicate the expected range of amplitudes for the cosmic strings, relic GW and supermassive black hole background respectively.

4. Results

Using the pulsar data-sets described above, the 95% detection rate upper bound with a false alarm rate of 0.1% is given in Table 3 for different values of α . The relationship between A and α is shown in Fig. 2. These upper bounds on A can be converted to an upper bound on the normalized GW energy-density per unit logarithmic frequency interval, $\Omega_{gw}(f)$ using equations 1 and 3. Our limits on $\Omega_{gw}(1\text{yr}^{-1})$ are indicated on the right-hand axis of Fig. 2.

We can compare our results to the previously published limit of Kaspi et al. (1994) who obtained that $\Omega_{gw}(1/8 \text{ yr})h^2 < 1.1 \times 10^{-7}$ (star symbol in Fig. 2). Using the same data-set as Kaspi et al. (1994) our method provides a similar limit of $\Omega_{gw}(1/8 \text{ yr})h^2 < 1.3 \times 10^{-7}$. Combining this data-set with our more recent observations provides a more stringent limit of $\Omega_{gw}(1/8 \text{ yr})h^2 < 1.9 \times 10^{-8}$.

The most stringent limit reported to date was obtained by Lommen (2002). Unfortunately, these observations are not publicly available. In order to compare our technique we use the original PSR B1855+09, Kaspi et al. (1994) data-set along with two simulated white data-sets that realistically model the NRAO 140-foot and Arecibo observations which form the remainder of the Lommen (2002) data (we simulate 60 observations with an rms residual of $5\mu\text{s}$ between MJDs 47800 and 51360 for the 140-foot telescope and a further 60 observations with an rms residual of $1\mu\text{s}$ between MJDs 50783 and 52609 for the most recent Arecibo data). As we simulate neither systematic effects nor timing noise our limit will be more stringent than could be obtainable using the real data-set. For $\alpha = -2/3$, we obtained that $A \leq 9 \times 10^{-15}$ corresponding to $\Omega_{gw}(1/17 \text{ yr})h^2 = 8 \times 10^{-9}$. This limit is a factor of four less stringent than that reported by Lommen (2002).

Using simulated data, the upper bounds that can be expected from future experiments can be determined. The goal of the PPTA is to time 20 pulsars with an rms timing residual of 100 ns over 5 years. The dashed line in Fig. 2 plots A versus α for such a data-set which could potentially provide a limit on a background of supermassive black hole systems of $A_{\text{upper}} < 6.5 \times 10^{-16}$ or $\Omega_{gw}(1/8 \text{ yr})h^2 \leq 6.6 \times 10^{-11}$ (see Table 3).

In Jenet et al. (2005), techniques to use an array of pulsars to detect a stochastic background of GWs with $\alpha = -2/3$ were developed.³ Given a value for A_{upper} , one can use such techniques to determine the probability of definitively detecting the GW background using the completed PPTA data-sets (20 pulsars with an rms timing residual of 100 ns over 5 years) if A were equal to A_{upper} . In terms of the parameter, S , defined in Jenet et al.

³Note that A as defined here is larger by a factor of $\sqrt{3}$ compared to the definition of A used in Jenet et al. (2005). The definition used here is consistent with Jaffe & Backer (2003) and Wyithe & Lobe (2003).

(2005), a significant detection would occur if $S > 3.1$. This corresponds to a 0.001 false alarm rate. For the case of $\alpha = -2/3$, the expected value of S (assuming ideal whitening) is about 4.1 for $A = A_{\text{upper}}$. Since the probability distribution of S is approximately Gaussian, the probability of $S > 3.1$ when $\langle S \rangle = 4.1$ is 85%. Hence, the GW background would be detected 85% of the time. For the case of 10 years of observations, the detection rate increases to over 99% of the time.

5. Implications and Discussion

The upper bound on the stochastic background can be used to probe several aspects of the Universe. Precisely what is being constrained depends on the physics of the particular background in question. Here, both the measured upper bounds using the currently available data and the expected upper bounds using the full five-year PPTA data-set are discussed in the context of several GW backgrounds.

5.1. Supermassive black holes

A GW background generated by an ensemble of supermassive black holes distributed throughout the universe has been investigated by several authors (Jaffe & Backer 2003, Wyithe & Loeb 2003, Enoki et al. 2004). In general, the characteristic strain spectrum for this background can be written as:

$$h_c(f) = 2.510^{-16} h \left(\frac{f}{\text{yr}^{-1}} \right)^{-2/3} \left\langle \left(\frac{M_c}{10^7 M_\odot} \right)^{5/3} \right\rangle^{1/2} \left(\frac{N_0}{\text{Mpc}^{-3}} \right)^{1/2} I^{1/2} \quad (8)$$

where

$$I = \int \frac{N(z)}{N_0} H_0 \frac{a(z)}{\dot{a}(z)} \frac{dz}{(1+z)^{4/3}}, \quad (9)$$

$a(z)$ is the cosmological scale factor written in terms of red shift, z , $\dot{a}(z)$ is the derivative of $a(z)$ with respect to cosmic time, H_0 is the Hubble constant, the chirp mass $M_c = [M_1 M_2 (M_1 + M_2)^{-1/3}]^{3/5}$ of a given binary system, $\langle \rangle$ represents ensemble averaging over all the systems generating the background, $N(z)$ is the galaxy merger rate as a function of red shift, and N_0 is the present day number density of merged galaxies that created a black-hole binary system. The values of each of these physical quantities are currently poorly constrained and each investigator has chosen a different parameterization. Under the framework described by Jaffe and Backer (2003), $\langle M_c^{5/3} \rangle$ and N_0 are constrained by observations at the current epoch to be $\langle M_c \rangle \approx 2.3 \times 10^7 M_\odot$ and $N_0 \approx 1/\text{Mpc}^3$. They

parameterized the galaxy merger rate such that $R(z)$ goes as $(1+z)^\gamma$. Hence, I depends on γ . Combining the estimates of $\langle M_c \rangle$ and N_0 together with our measured upper bound of $A_{\text{upper}} = 1.1 \times 10^{-14}$, one finds that $I \leq 3$. Using the full PPTA after 5 years, one expects $I \leq 0.8$. These constraints together with the calculations of Jaffe & Backer (2003) (see Fig. 4 in their work) constrain γ . Currently the limit on γ is < 2.6 and with the full PPTA $\gamma < 0.4$. This value is expected to lie somewhere between -0.4 and 2.3 (Carlberg et al. 2000, Patton et al. 2002). Current PPTA sensitivity (i.e. using the data presented in this paper) is just above the expected range, while the full PPTA should be able to place meaningful constraints on this exponent.

In the Wyithe & Loeb (2003) work, both $\langle M_c^{5/3} \rangle$ and I depend strongly on the black-hole versus galactic-halo mass ($M_{\text{BH}} - M_{\text{HM}}$) relationship. They discuss several different scenarios which yield different $M_{\text{BH}} - M_{\text{HM}}$ relationships and hence different levels of the background. For the case of an $M_{\text{BH}} - M_{\text{HM}}$ relationship determined by Ferrarese (2002), the expected value of A is 2×10^{-15} . For the $M_{\text{BH}} - M_{\text{HM}}$ relationship derived from Navarro, Frenk, & White (1997), $A = 5 \times 10^{-15}$. Using an $M_{\text{BH}} - M_{\text{HM}}$ relationship derived from simple considerations of BH growth by feedback from quasar activity (Wyithe & Loeb 2003, Haehnelt, Natarajan & Rees 1998, Silk & Rees 1998), $A \approx 10^{-15}$. Our measured upper limit for $\alpha = -2/3$ cannot rule out any of these models. However, if only a limit is obtained from the full PPTA observations, it will rule out all of the models described above.

5.2. Relic gravitational waves

A relic gravitational wave background is generated by the interaction between the large-scale dynamic cosmological metric and quantum fluctuations of the metric perturbations occurring in the early universe (Grishchuk 2005). In the nano-Hz frequency regime, the background takes the following form:

$$h_c(f) = h_c(f_h) \left(\frac{f}{H_0} \right)^\alpha \left(\frac{a_2}{a_H} \right)^{\frac{1}{2}} \quad (10)$$

where $h_c(f_h)$ is the magnitude of the characteristic strain spectrum at $f = H_0$, a_H is the current value of the cosmological expansion factor, and a_2 is the value of the expansion factor at the start of the matter-dominated epoch. Note that this expression is not valid in the ultra-low frequency regime where $f \approx H_0$. The notation used here is consistent with Grishchuk (2005) except for α which is related to Grishchuk's parameter β by $\alpha = 1 + \beta$. The exponent determines the evolution of the inflationary epoch which starts the GW amplification process. When $\alpha = -1$, the scale factor grows exponentially with global cosmic time. The ratio a_2/a_H is believed to be about 10^{-4} . $h_c(f_h)$ is constrained by cosmic

microwave background measurements to be about 10^{-5} . Using these values and assuming the validity of the amplification scenario described in Grishchuk (2005), the upper bound on A may be used to constrain α . The upper bound on α is given by the solution to the following equation:

$$h_c(f_h) \left(\frac{1/1 \text{ yr}}{f_h} \right)^\alpha \left(\frac{a_2}{a_H} \right)^{\frac{1}{2}} = A(\alpha). \quad (11)$$

The above equation yields $\alpha \leq -0.7$ for the current PPTA and $\alpha \leq -0.84$ for the full PPTA. Within the theoretical framework described by Grishchuk (2005), if α is larger than -0.80 , small scale gravitational waves will effect primordial nucleosynthesis, while an α less than -1.0 will result in an infinitely large energy density in small scale gravitational waves. Hence, the full PPTA will be able to place useful constraints on the relic gravitational wave background. Since α determines the rate of expansion in the inflationary epoch, it turns out that it is related to the equation of state of the “matter” in that epoch by

$$\frac{P}{\epsilon} = w = \frac{2 - \alpha}{3\alpha}. \quad (12)$$

where P is the pressure and ϵ the energy density. The full PPTA will constrain w in the early universe to be greater than -1.17 . This would limit inflationary models based on “quintessence” and “phantom energy” (Nojiri et al. 2006; Padmanabhan 2005).

5.3. Cosmic strings

It has been proposed that oscillating cosmic string loops will produce gravitational wave radiation (Vilenkin 1981). Recently, Damour & Vilenkin (2005) discussed the possibility of generating a stochastic GW background using a network of cosmic superstrings. Using a semi-analytical approach, they derived the following characteristic strain spectrum valid in the pulsar timing frequency range (see their equation 4.8):

$$h_c(f) = 1.6 \times 10^{-14} c^{1/2} p^{-1/2} \epsilon_{eff}^{-1/6} (h/.65)^{7/6} \left(\frac{G\mu}{10^{-6}} \right)^{1/3} \left(\frac{f}{\text{yr}^{-1}} \right)^{-7/6} \quad (13)$$

where μ is the string tension, G is Newton’s constant, c is the average number of cusps per loop oscillation, p is the reconnection probability, ϵ_{eff} is a loop length scale factor, and h is the Hubble constant in units of 100 km/s/Mpc. Note that for the above estimate, h was evaluated at 0.65 in order to be consistent with Damour & Vilenkin (2005). The combination $G\mu$ is the dimensionless string tension which characterizes the gravitational interaction of the strings. The predicted string tensions are $10^{-11} \leq G\mu \leq 10^{-6}$ (Damour & Vilenkin 2005).

Using the above spectrum together with the measured upper bound on h_c for $\alpha = -7/6$, an upper bound may be placed on the dimensionless string tension:

$$G\mu \leq 1.5 \times 10^{-8} c^{-3/2} p^{3/2} \epsilon_{eff}^{1/2} (h/.65)^{-7/2}. \quad (14)$$

As emphasized by Damour & Vilenkin (2005), the above expression for the upperbound may be simplified using the fact that both p and ϵ_{eff} are less than one and h is expected to be greater than .65:

$$G\mu \leq 1.5 \times 10^{-8} c^{-3/2}. \quad (15)$$

Using standard model assumption where $c = 1$, the upperbound becomes $G\mu \leq 1.5 \times 10^{-8}$. This is already limiting the parameter space of the cosmic string model of Sarangi and Tye (2002). With the full PPTA, the limit will become $G\mu \leq 5.36 \times 10^{-12}$. Hence, the full PPTA will either detect GWs from cosmic strings or rule out most current models.

Acknowledgments

The authors would like to thank J. Armstrong, T. Damour, and L. P. Grishchuck for contributing valuable advice during the preparation of this manuscript. Some of the data presented in this paper were obtained as part of the Parkes Pulsar Timing Array project which is a collaboration between the ATNF, Swinburne University and The University of Texas, Brownsville. We thank our collaborators on this project. The Parkes radio telescope is part of the Australia Telescope which is funded by the Commonwealth of Australia for operation as a National Facility managed by CSIRO. Part of this research was supported by NASA under grant NAG5-13396 and the National Science Foundation under grant AST-0545837.

REFERENCES

- Abbott, B., Abbott, R., Adhikari, R. et al. 2006, Phys. Rev. D, 73, 062001
- Bertotti, B., Carr, B. J., & Rees, M. J. 1983, MNRAS, 203, 945
- Carlberg, R. G., Cohen, J. G., Patton, D. R. et al., A. 2000, ApJ, 532, L1
- Damour, T. & Vilenkin, A. 2005, Phys. Rev. D, 71, 063510
- Detweiler, S. 1979, ApJ, 234, 1100
- Edwards, R. T., Hobbs, G. B., & Manchester, R. N. 2006, MNRAS, submitted

- Enoki, M., Inoue, K. T., Nagashima, M., & Sugiyama, N. 2004, *ApJ*, 615, 19
- Ferrarese, L. 2002, *ApJ*, 578, 90
- Foster, R. S. & Backer, D. C. 1990, *ApJ*, 361, 300
- Grishchuk, L. P. 2005, *Physics-Uspekhi*, 48, 1235
- Haehnelt, M. G., Natarajan, P., & Rees, M. J. 1998, *MNRAS*, 300, 817
- Hobbs, G. 2005, *PASA*, 22, 179
- Hobbs, G. B., Edwards, R. T., & Manchester, R. N. 2006, *MNRAS*, in press
- Hotan, A. W., Bailes, M., & Ord, S. M. 2006, *MNRAS*
- Jaffe, A. H. & Backer, D. C. 2003, *ApJ*, 583, 616
- Jenet, F. A., Hobbs, G. B., Lee, K. J., & Manchester, R. N. 2005, *ApJ*, 625, L123
- Kaspi, V. M., Taylor, J. H., & Ryba, M. 1994, *ApJ*, 428, 713
- Lommen, A. N. 2002, in *WE-Heraeus Seminar on Neutron Stars, Pulsars, and Supernova Remnants*, ed. W. Becker, H. Lesch, & J. Trümper (Garching: Max-Planck-Institut für Extraterrestrische Physik), 114–125
- Lorimer, D. R. and Kramer, M. 2005, *Handbook of Pulsar Astronomy* (Cambridge University Press)
- Maggiore, M. 2000, *Phys. Rep.*, 331, 283
- McHugh, M. P., Zalamansky, G., Verotte, F., & Lantz, E. 1996, *Phys. Rev. D*, 54, 5993
- Navarro, J. F., Frenk, C. S., & White, S. D. M. 1997, *ApJ*, 490, 493
- Nojiri, S., Odintsov, S. D., & Gorbunova, O. G. 2006, *J. Phys.*, A39, 6627
- Padmanabhan, T. 2005, in , *proc. 29th Int. Cosmic Ray Conf., Pune, India*, in press. (astro-ph/0510492)
- Patton, D. R., Pritchett, C. J., Carlberg, R. G. et al., 2002, *ApJ*, 565, 208
- Sazhin, M. V. 1978, *Sov. Astron.*, 22, 36
- Sesana, A., Haardt, F., Madau, P., & Volonteri, M. 2004, *ApJ*, 611, 623

Silk, J. & Rees, M. J. 1998, *A&A*, 331, L1

Thorsett, S. E. & Dewey, R. J. 1996, *Phys. Rev. D*, 53, 3468

Vilenkin, A. 1981, *Phys Lett B*, 107, 47

Wyithe, J. S. B. & Loeb, A. 2003, *ApJ*, 590, 691

Table 3: Current and potential future limits on the stochastic gravitational-wave background

α	A	$\Omega_{gw}(1/1 \text{ yr})h^2$	$\Omega_{gw}(1/8 \text{ yr})h^2$	$\Omega_{gw}(1/20 \text{ yr})h^2$
-2/3	1.1×10^{-14}	7.6×10^{-8}	1.9×10^{-8}	1.0×10^{-8}
-1	5.7×10^{-15}	2.0×10^{-8}	2.0×10^{-8}	2.0×10^{-8}
-7/6	3.9×10^{-15}	9.6×10^{-9}	1.9×10^{-8}	2.6×10^{-8}
-2/3	6.5×10^{-16}	2.7×10^{-10}	6.6×10^{-11}	3.6×10^{-11}
-1	3.8×10^{-16}	9.1×10^{-11}	9.1×10^{-11}	9.1×10^{-11}
-7/6	2.8×10^{-16}	4.9×10^{-11}	9.9×10^{-11}	1.3×10^{-10}

Note. — The upper half of the table gives limits derived from current observations. Limits based on timing 20 pulsars with an rms timing residual of 100 ns over 5 yr are given in the lower half of the table.